Available online at www.sciencedirect.com

ScienceDirect

Advances in Space Research 71 (2023) 803–815

ADVANCES IN SPACE RESEARCH (a COSPAR publication)

www.elsevier.com/locate/asr

Active shape control for flexible space structures using an optimal gyricity distribution

Xiaoyu Lang [a,b,c,*], Christopher J. Damaren [b]

[a] Beijing Institute of Technology, School of Automation, No. 5, South Street, Zhongguancun, Haidian District, Beijing 100081, China
[b] University of Toronto Institute for Aerospace Studies, 4925 Dufferin Street, Toronto, Ontario M3H 5T6, Canada
[c] Harbin Institute of Technology, Research Center of Satellite Technology, Yikuang Street #2, Harbin 150080, China

Received 25 June 2022; received in revised form 21 September 2022; accepted 21 October 2022
Available online 28 October 2022

Abstract

An active shape control approach for a circular flexible space structure is studied. The shape of these flexible structures may need active shape control due to some particular mission objectives. For example, antenna reflectors may have requirements for their shape accuracy to guarantee communication performance; and some solar sails may change their shape to realize different commissions during interplanetary flight. This paper investigates an active shape control process executed by the gyricity (stored angular momentum) distribution existing in the circular flexible space structure. The shape of the circular flexible space structure is expected to be reformed from a plane plate to a paraboloidal plate. An optimal gyricity distribution is derived based on the optimal control theory for systems described by partial differential equations. Distributed forces can be generated by the optimal gyricity distribution in a rotating field to implement the active shape control. The dynamic model of the circular flexible space structure is established for the active shape control through the finite element method. Numerical simulation validates the functionality of the shape control method, and illustrates the shape-adjusting process of the circular flexible space structure.

Keywords: Active shape control; Gyricity distribution; Flexible space structure

1. Introduction

Large flexible space structures (LFSS), such as solar sails, solar arrays, antennas, etc., are commonly used in space applications. The shape of LFSS is of importance to realize their functionalities and even to improve their performance, which makes active shape control worth studying. For solar arrays and antennas, their shape deformation may be passively incurred by the changing thermal environment at different positions in their orbits. The active shape control in these scenarios implements precise control to suppress the deformation or attenuate vibrations of the flexible structures (Tabata and Natori, 1996). For solar sails, active shape control can be used to change its shape to attain different purposes which was proposed in Borggräfe et al. (2013) and its basic idea is sketched in Fig. 1. When the solar sail sets out from the Earth, the shape remains a plane plate to obtain as much thrust from solar pressure as possible (Fig. 1(a)). When the solar sail is approaching the target destination like asteroids, the shape is deformed to be a paraboloidal plate such that the solar sail can serve as an antenna reflector (Fig. 1(b)) or an energy collector (Fig. 1(c)). When its shape becomes unsymmetrical, torques for attitude control can be generated from differential thrusts, as shown in Fig. 1(d).

* Corresponding author at: Beijing Institute of Technology, School of Automation, No. 5, South Street, Zhongguancun, Haidian District, Beijing 100081, China.
E-mail address: xylang@bit.edu.cn (X. Lang).

https://doi.org/10.1016/j.asr.2022.10.049
0273-1177/

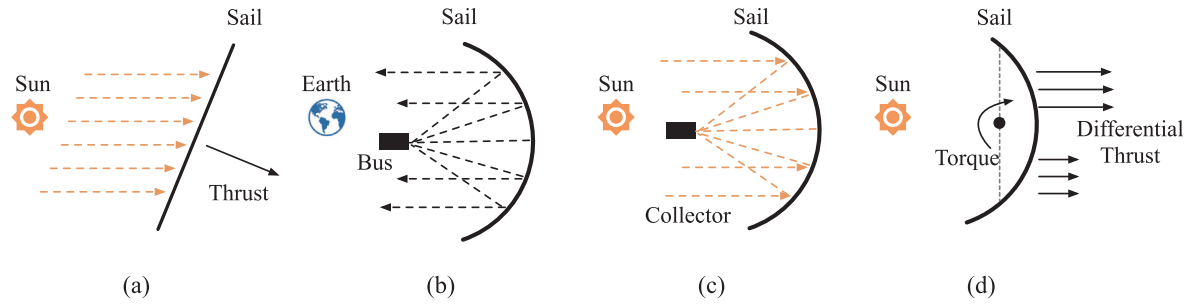

Fig. 1. Multi-functional platform of solar sail (Borggräfe et al., 2013): (a) thrust mode; (b) reflector mode; (c) energy collector; (d) a.ttitude control.

Active shape control methods for LFSS have been extensively studied by many researchers. An optimal quasi-static shape control scheme was proposed by Balas (1985) for large space structures to track a desired shape. Internal translational actuators were used by Austin et al. (1994) to design a static shape control scheme for flexible structures. The shape control of a gossamer space reflector structure was analyzed using large arrays of distributed actuators (Gorinevsky et al., 2001). An active robust shape control method was developed by Hu and Vukovich (2005) to deal with parameter perturbation uncertainty. Heaters were employed by Zhang et al. (2013) for the quasi-static shape control of flexible space structures to minimize the control energy cost. H_∞ feedback control was provided by Xie et al. (2016) for the dynamic shape control of deployable mesh reflectors in different temperature zones. An active shape adjustment scheme for a large cable-mesh reflector was addressed in Xun et al. (2018) using piezoceramic actuators. Wrinkles distortion was analyzed by Fan et al. (2020) to show its effects on electromagnetic performance of an active membrane phased array antenna. Liu et al. (2021) used the reflectivity control devices to modulate the solar radiation pressure to control the shape of reflectors. Topology optimization was utilized to preserve the shape of a flexible structure (Silva et al., 2021). Zhou et al. (2021) developed an integrated design approach for active shape morphing of piezo-actuated wings. The shape of a spinning membrane can be changed by exciting the static wave to achieve large deformation (Takao et al., 2022). Different from the above mentioned research results, which were based on the special material properties of the flexible space structures, the concept of a gyroelastic continua is possibly an alternative artifice for the shape control of large flexible space structures (D'Eleuterio and Hughes, 1987). This concept was proposed by D'Eleuterio and Hughes (1984) in which the flexible structure is considered as a continuous distribution of mass, stiffness and gyricity (stored angular momentum). The identities satisfied by modal parameters for a gyroelastic continuum were presented by Hughes and D'Eleuterio (1986). The dynamic motion of spacecraft with a number of gyric flexible appendages was analyzed by D'Eleuterio and Hughes (1987). An optimal problem for distributed gyricity was explored for the shape control of large space structures (Damaren and D'Eleuterio, 1989). The conditions of controllability and observability for gyroelastic flexible structures were discussed by Damaren and D'Eleuterio (1991). The vibration of large space structure can be attenuated with an optimal gyricity distribution using a collection of control moment gyros (Chee and Damaren, 2015). The dynamics of gyroelastic Euler–Bernoulli beams were extended to Timoshenko beams by Hassanpour and Heppler (2016), and a numerical comparison between these two kinds of beams were made to present the difference. This paper is concerned with the theory of gyroelastic continuum to design an active shape control scheme for a large flexible circular space structure. An optimal gyricity distribution is derived from the optimization theory for systems governed by partial differential equations to control the structural shape, which is the main contribution of this paper. The shape of this structure is expected to be changed from a plane plate to a paraboloidal plate using such an optimal gyricity distribution derived from the optimization theory of systems governed by partial differential equations. Note that the optimality in this paper refers to the most favorable gyricity distribution which is used to change the shape of the flexible space structure from a plain plate to a paraboloidal plate.

The reminder of this paper is as follows. In Section 2, some fundamental knowledge about gyroelastic continua is reviewed and the problem studied in this paper is introduced. In Section 3, the optimal gyricity distribution is derived from the optimal theory about systems governed by partial differential equations. The dynamic process of the active shape control is illustrated by numerical simulations in Section 4. Some conclusions are remarked in Section 5.

2. Preliminaries

2.1. Gyricity distribution

This paper selects a circular plate to represent a flexible space structure. As a general shape, a circular shape is a general centrally symmetric and appears in many typical space flexible structures, such as solar sails (Hu et al., 2016), space antennas (Sanz-Fernandez et al., 2015), etc. The functions of these space structures can also be realized by a single body with multiple shapes corresponding to

multiple functions, as suggested by Borggräfe et al. (2013). A circular flexible space structure is simply sketched in Fig. 2. Take an arbitrary point of this structure. The position vector of this point is $\boldsymbol{r} = [x, y, z]^\top$, which is expressed in the local reference frame originated at the center of the flexible structure. This point's total displacement $\boldsymbol{w}(\boldsymbol{r}, t)$ can be written as

$$\boldsymbol{w}(\boldsymbol{r}, t) = \boldsymbol{w}_0 - \boldsymbol{r}^\times \boldsymbol{\theta} + \boldsymbol{u}_e(\boldsymbol{r}, t) \tag{1}$$

where $\boldsymbol{w}_0$ is the translation of the origin point O, $\boldsymbol{\theta} = [\theta_1, \theta_2, \theta_3]^\top$ is the small rotation of this flexible space structure, and $\boldsymbol{u}_e$ is the small elastic deformation at $\boldsymbol{r}$. Note that the vector $\boldsymbol{\theta}$ is the small angle approximation of the Euler angles used in the direction cosine matrix, namely $\boldsymbol{C} \approx \boldsymbol{1} - \boldsymbol{\theta}^\times$. The notation $(\cdot)^\times$ represents the skew symmetric matrix of an arbitrary vector $\boldsymbol{a} = [a_1, a_2, a_3]^\top$ and is given by:

$$\boldsymbol{a}^\times = \begin{bmatrix} 0 & -a_3 & a_2 \\ a_3 & 0 & -a_1 \\ -a_2 & a_1 & 0 \end{bmatrix} \tag{2}$$

The structural dynamics are given by (D'Eleuterio and Hughes, 1984; Damaren and D'Eleuterio, 1989; Damaren and D'Eleuterio, 1991):

$$\mathcal{M}\ddot{\boldsymbol{w}} + \mathcal{G}\dot{\boldsymbol{w}} + \mathcal{K}\boldsymbol{w} = \mathcal{F} \tag{3}$$

Here, $\mathcal{M}$ is the self-adjoint mass operator and specified as $\mathcal{M} = \rho(\boldsymbol{r})\boldsymbol{1}$, where $\rho(\boldsymbol{r})$ is the mass density at $\boldsymbol{r}$ and $\boldsymbol{1}$ is the identity operator, and $\mathcal{K}$ is the self-adjoint stiffness operator. The external force is denoted by $\mathcal{F}$. The term $\mathcal{G}$ is called gyricity operator which is given by:

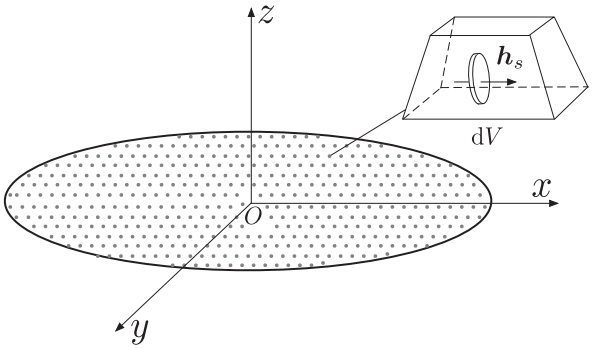

Fig. 2. Circular gyroelastic space flexible structure.

$$\mathcal{G} = -\frac{1}{4}\nabla^\times \boldsymbol{h}_s^\times \nabla^\times \tag{4}$$

where the term ∇ is the gradient operator, and $\boldsymbol{h}_s(\boldsymbol{r})$ is called the gyricity distribution of the structure at $\boldsymbol{r}$ which indicates the stored angular momentum in each unit volume of the flexible space structure, as shown in Fig. 2. Note that the gyricity distribution is assumed to be continuous in order to yield the optimal gyricity distribution for structure's shape control. In practice, the continuous gyricity distribution can be realized by discrete distribution using a limited number of wheels embedded into the flexible structure, which has already been discussed by Damaren and D'Eleuterio (1991, 2015) and hence is omitted in this paper.

2.2. Problem statement

Assume that the circular flexible space structure is imbued with a continuous gyricity distribution. When the circular flexible space structure is rotating, the shape of the structure is aiming to be deformed from a plane-plate shape to a paraboloidal shape using the gyricity distribution, as depicted in Fig. 3 (This figure is the projection of the $x - z$ plane of Fig. 2). Specifically, the circular flexible space structure is assumed to be rotating about its z-axis by the angular velocity Ω. The final objective shape of the circular flexible space structure is expected to be a paraboloid. This indicates that the vertical displacement w_e^* of the point at the radius r in the final objective stage is given by:

$$w_e^* = Cr^2 \tag{5}$$

where C is a constant. Essentially, the forces produced by the rotating gyricity distribution balance out the stiffness forces due to elasticity. The objective is to determine an optimal gyricity distribution which can render the shape control of the flexible structure.

3. Optimal gyricity distribution

The circular flexible space structure shown in Fig. 2 is now projected on the $x - y$ plane for illustrating the notion of the gyricity distribution, as depicted in Fig. 4. The small circle with an arrow in Fig. 4 represents a nominal wheel which can generate angular momentum. The positive direction of the angular momentum is assumed to be from the

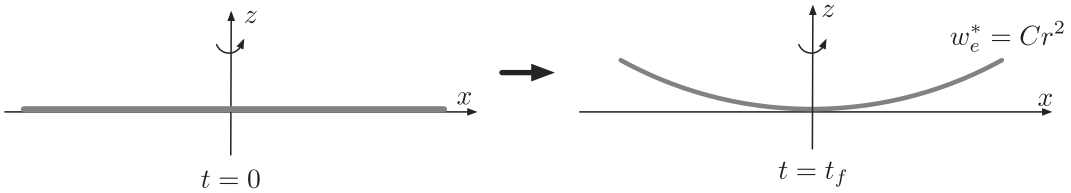

Fig. 3. Diagram for the shape deformation of the flexible space structure.

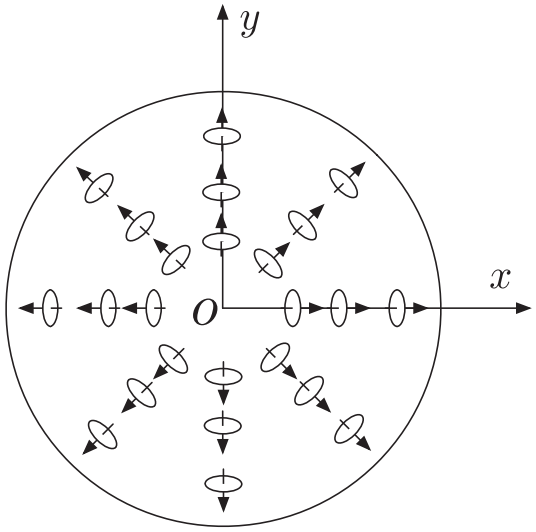

Fig. 4. Diagram for gyricity distribution.

circular flexible space structure's central point to its edge along the radial direction.

Recall the total displacement $\boldsymbol{w}(\boldsymbol{r},t)$ in Eq. (1). Taking the derivative and second-order derivative of $\boldsymbol{w}(\boldsymbol{r},t)$ with respect to time gives

$$\begin{aligned}\dot{\boldsymbol{w}} &= -\boldsymbol{r}^{\times}\dot{\boldsymbol{\theta}} + \dot{\boldsymbol{u}}_e \\ \ddot{\boldsymbol{w}} &= -\boldsymbol{r}^{\times}\ddot{\boldsymbol{\theta}} + \ddot{\boldsymbol{u}}_e\end{aligned} \tag{6}$$

where the translation $\boldsymbol{w}_0$ is regarded as a constant. The circular flexible space structure is expected to rotate about its z-axis by the angular velocity Ω, it means $\dot{\boldsymbol{\theta}} = [0,0,\Omega]^{\top}$ and $\ddot{\boldsymbol{\theta}} = \boldsymbol{0}$. Assume that only the elastic deformation in z-axis (vertical displacement), w_e, is considered here such that $\boldsymbol{u}_e = [0,0,w_e]^{\top}$. Taking $\boldsymbol{u}_e$ to be a small displacement, we have $\dot{\boldsymbol{u}}_e = \boldsymbol{0}$ and $\ddot{\boldsymbol{u}}_e = \boldsymbol{0}$. When the external force $\mathcal{F}$ is not considered, Eq. (3) can be simplified as:

$$\mathcal{G}\dot{\boldsymbol{w}} + \mathcal{K}\boldsymbol{w} = \boldsymbol{0} \tag{7}$$

Remark 1. Note that Eq. (7) is the fundamental equation to obtain the optimal gyricity distribution for the shape control of the circular flexible space structure. The shape deformation is triggered by the equilibrium between the structure's stiffness (related to $\mathcal{K}$ in Eq. (7)) and the distributed forces produced by the gyricity distribution $\boldsymbol{h}_s$(related to $\mathcal{G}$ in Eq. (7)) in a rotating field (The structure is rotating about its z-axis with the angular velocity Ω). The gyricity distribution is actually the source of control force to implement shape deformation.

According to the Kirchhoff plate theory (Timoshenko and Woinowsky-Krieger, 1959), the stiffness operator $\mathcal{K}$ is given by:

$$\mathcal{K} = D\nabla^2\nabla^2, \qquad D = \frac{h^3E}{12(1-\nu^2)} \tag{8}$$

where h is the thickness of the plate, E is the elastic modulus, and ν is the Poisson's ratio. Given that the flexible space structure is circular, cylindrical coordinates are much easier to formulate the structural dynamics compared with the Cartesian coordinates. Notice that the operator $\nabla^{\times}$ in Cartesian coordinates satisfies the skew-symmetric property $\nabla^{\times} = -(\nabla^{\times})^{\top}$. But this property is not held by $\nabla^{\times}$ in cylindrical coordinates. Thus, the operator $\nabla^{\times}$ is renamed as **curl** in cylindrical coordinates and it is given by:

$$\mathbf{curl} = \begin{bmatrix} 0 & -\frac{\partial}{\partial z} & \frac{1}{r}\frac{\partial}{\partial \theta} \\ \frac{\partial}{\partial z} & 0 & -\frac{\partial}{\partial r} \\ -\frac{1}{r}\frac{\partial}{\partial \theta} & \frac{1}{r}\frac{\partial}{\partial r}(r\cdot) & 0 \end{bmatrix} \tag{9}$$

As mentioned before, the distributed nominal wheels (shown in Fig. 4) can produce the radial gyricity distribution (radial angular momentum distribution) h_r whose direction is starting from the central point of the flexible structure to its edge. Hence, $\boldsymbol{h}_s$ can be expressed in the cylindrical coordinate as:

$$\boldsymbol{h}_s = \begin{bmatrix} h_r(r) \\ 0 \\ 0 \end{bmatrix} \tag{10}$$

Substituting Eqs. (4), (8), and (10) into Eq. (7), the subsequent result can be simplified to give

$$D\frac{\partial^4 w_e}{\partial r^4} = \Omega\left(\frac{1}{r} + \frac{\partial}{\partial r}\right)h_r \tag{11}$$

Since the circular flexible space structure shown in Fig. 4 is centrally symmetric, Eq. (11) is formulated in a scalar form. From Eq. (11), it can be noticed that this is a partial differential equation with respect to the state, namely the vertical displacement w_e. The radial gyricity distribution h_r can be regarded as the equivalent control input of this partial differential equation [Eq. (11)] governing the flexible structure system, which is compatible with the optimal control theory for systems described by partial differential equations (Lions, 1971). Hence, Eq. (11) can be rewritten as

$$\mathcal{A}w_e = \mathcal{B}h_r \tag{12}$$

where

$$\mathcal{A} = \frac{D}{\Omega}\frac{\partial^4}{\partial r^4}(\cdot), \qquad \mathcal{B} = \left(\frac{1}{r} + \frac{\partial}{\partial r}\right)(\cdot) \tag{13}$$

A tiny-size hole is set at the central point of the circular structure to avoid the potential singularity issue due to the term $1/r$. Define an objective function as

$$\mathcal{J} = \int_{r_h}^{R}\{(w_e - Cr^2)^2 + Nh_r^2\}\mathrm{d}r \tag{14}$$

where r_h is the radius of the central hole and R is the outer radius of the flexible space structure. C and N in Eq. (14) are two positive constants, where C is the coefficient of

the paraboloidal shape (Cr^2) and N is the weight parameter defined in the objective function. The selections of both constants depend on the specific practical situation. Denote an admissible control set $\mathcal{U}_{ad}$(this is the set of square-integrable functions on $[r_h, R]$). The problem studied in this paper can be elaborated as: find an optimal radial gyricity distribution h_r^* such that

$$\mathcal{J}(h_r^*) = \min_{h_r \in \mathcal{U}_{ad}} \mathcal{J}(h_r) \tag{15}$$

In order to solve this optimization problem, we select an adjoint state $p(h_r)$ to formulate an adjoint state equation:

$$\mathcal{A}^* p(h_r) = w_e - Cr^2 \tag{16}$$

where $\mathcal{A}^*$ is the adjoint operator of $\mathcal{A}$ and its form is given by

$$\mathcal{A}^* = \frac{D}{\Omega}\frac{\partial^4}{\partial r^4}(\cdot) = \mathcal{A}, \tag{17}$$

i.e. $\mathcal{A}$ is self-adjoint. According to the optimal control theory of systems governed by partial differential equations (Lions, 1971), the solution of the optimal problem shown in Eq. (15) is expressed as:

$$h_r^* = -N^{-1}\mathcal{B}^* p \tag{18}$$

where $\mathcal{B}^*$ is the adjoint operator of $\mathcal{B}$ which is given by

$$\mathcal{B}^* = \left(\frac{1}{r} - \frac{\partial}{\partial r}\right)(\cdot) \tag{19}$$

Substituting Eq. (19) into Eq. (18), one can have

$$h_r^* = -N^{-1}\frac{1}{r}p + N^{-1}\frac{\partial p}{\partial r} \tag{20}$$

Substituting the above result into Eq. (11) yields

$$\begin{aligned}
\tfrac{D}{\Omega}\tfrac{\partial^4 w_e}{\partial r^4} &= \left(\tfrac{1}{r} + \tfrac{\partial}{\partial r}\right)h_r^* \\
&= \left(\tfrac{1}{r} + \tfrac{\partial}{\partial r}\right)\left(-N^{-1}\tfrac{1}{r}p + N^{-1}\tfrac{\partial}{\partial r}p\right) \\
&= -\tfrac{1}{r^2}N^{-1}p + \tfrac{1}{r}N^{-1}\tfrac{\partial p}{\partial r} - N^{-1}\tfrac{\partial}{\partial r}\left(\tfrac{1}{r}p\right) + N^{-1}\tfrac{\partial}{\partial r}\left(\tfrac{\partial p}{\partial r}\right) \\
&= -\tfrac{1}{r^2}N^{-1}p + \tfrac{1}{r}N^{-1}\tfrac{\partial p}{\partial r} + \tfrac{1}{r^2}N^{-1}p - \tfrac{1}{r}N^{-1}\tfrac{\partial p}{\partial r} + N^{-1}\tfrac{\partial}{\partial r}\left(\tfrac{\partial p}{\partial r}\right) \\
&= N^{-1}\tfrac{\partial^2 p}{\partial r^2}
\end{aligned} \tag{21}$$

This implies that

$$\frac{D}{\Omega}\frac{\partial^4 w_e}{\partial r^4} = N^{-1}\frac{\partial^2 p}{\partial r^2} \tag{22}$$

Recalling Eq. (16), the adjoint state equation can be written as

$$\frac{D}{\Omega}\frac{\partial^4 p}{\partial r^4} = w_e - Cr^2 \tag{23}$$

In Eq. (22), taking partial derivatives twice with respect to r gives

$$\frac{\partial^2}{\partial r^2}\left(\frac{D}{\Omega}\frac{\partial^4 w_e}{\partial r^4}\right) = \frac{\partial^2}{\partial r^2}\left(N^{-1}\frac{\partial^2 p}{\partial r^2}\right) \tag{24}$$

Thus,

$$\frac{D}{\Omega}\frac{\partial^6 w_e}{\partial r^6} = N^{-1}\frac{\partial^4 p}{\partial r^4} \tag{25}$$

Substituting Eq. (23) into Eq. (25) yields an ordinary differential equation:

$$\frac{D}{\Omega}\frac{\partial^6 w_e}{\partial r^6} - \frac{\Omega}{D}N^{-1}w_e = -\frac{\Omega}{D}N^{-1}Cr^2 \tag{26}$$

The characteristic equation of Eq. (26) is given by:

$$\lambda^6 - \frac{\Omega^2 N^{-1}}{D^2} = 0 \tag{27}$$

The roots of Eq. (27) can be written as

$$\lambda_n = \nu_n + \mu_n \mathrm{i}(n = 1, 2, \cdots, 6) \tag{28}$$

where i is the imaginary unit. Hence, the solution of Eq. (26) is given by

$$\begin{aligned}
w_e = {} & C_1 e^{\nu_1 r}\cos(\mu_1 r) + C_2 e^{\nu_2 r}\sin(\mu_2 r) + C_3 e^{\nu_3 r}\cos(\mu_3 r) + \\
& C_4 e^{\nu_4 r}\sin(\mu_4 r) + C_5 e^{\nu_5 r}\cos(\mu_5 r) + C_6 e^{\nu_6 r}\sin(\mu_6 r) + Cr^2
\end{aligned} \tag{29}$$

where $C_1, C_2, \cdots, C_6$ are six constant numbers which will be determined by the boundary conditions governing Eq. (26). The boundary conditions for Eq. (26) are set as

$$\begin{aligned}
w_e(r_h) = w_e'(r_h) = w_e''(R) = w_e'''(R) = w_e^{(4)}(R) \\
= w_e^{(5)}(R) = 0
\end{aligned} \tag{30}$$

where r_h is the radius of the central hole and R is the outer radius of the flexible structure. The reason why the boundary condition is given at $w_e(r_h)$ instead of $w_e(0)$ is to avoid the singularity issue due to the term $1/r$ in Eq. (20). Note that the boundary conditions in Eq. (30) are set to obtain the six constants in Eq. (29) mathematically. As Remark 1 indicates, the shape deformation is attained by the equilibrium between the structure's stiffness and the distributed forces created by the gyricity at every time instant of the entire shape control process, which has no direct tie to the boundary conditions. Then, substituting Eq. (29) and the constants $C_1, C_2, \cdots, C_6$ into Eq. (23) gives

$$\begin{aligned}
\tfrac{D}{\Omega}\tfrac{\partial^4 p}{\partial r^4} &= C_1 e^{\nu_1 r}\cos(\mu_1 r) + C_2 e^{\nu_2 r}\sin(\mu_2 r) + C_3 e^{\nu_3 r}\cos(\mu_3 r) + \\
&\quad C_4 e^{\nu_4 r}\sin(\mu_4 r) + C_5 e^{\nu_5 r}\cos(\mu_5 r) + C_6 e^{\nu_6 r}\sin(\mu_6 r) \\
&= (*)
\end{aligned} \tag{31}$$

Integrating both sides of Eq. (31) four times gives

$$\begin{aligned}
\tfrac{D}{\Omega}p''' &= \textstyle\int(*) + C_{p1} \\
\tfrac{D}{\Omega}p'' &= \textstyle\int\int(*) + C_{p1}r + C_{p2} \\
\tfrac{D}{\Omega}p' &= \textstyle\int\int\int(*) + \tfrac{1}{2}C_{p1}r^2 + C_{p2}r + C_{p3} \\
\tfrac{D}{\Omega}p &= \textstyle\int\int\int\int(*) + \tfrac{1}{6}C_{p1}r^3 + \tfrac{1}{2}C_{p2}r^2 + C_{p3}r + C_{p4}
\end{aligned} \tag{32}$$

where C_{p1}, C_{p2}, C_{p3}, and C_{p4} are four constant numbers which will be determined by the boundary conditions governing Eq. (23). These boundary conditions are set as:

$$p(r_h) = p'(r_h) = p(R) = p'(R) = 0 \tag{33}$$

When the constants C_{p1}, C_{p2}, C_{p3}, and C_{p4} are calculated, substituting Eq. (32) into Eq. (20) gives the final result of the optimal solution h_r^*.

Since the analytic form of the optimal solution h_r^* is fairly complicated, a graphical depiction of this solution is given instead. Select the constant parameters for presenting h_r^* as: $N = 1 \times 10^{-7}, \Omega = 2\pi \text{rad/s}, C = 0.02$. The optimal gyricity distribution h_r^* is depicted in Fig. 5.

Remark 2. The small rotation $\boldsymbol{\theta}$ is only used in Section 3 to facilitate the calculation the optimal gyricity distribution. This restriction will be relaxed as full-angle rotation in the subsequent sections since it is the real case of flexible space structure operating in space.

4. Active shape control for circular flexible structures with an optimal gyricity distribution

Recalling Fig. 3, the aim of this paper is to change the shape of the circular flexible space structure from a plane plate to a paraboloidal plate. From Section 3, the optimal gyricity distribution h_r^* has already been obtained using the optimal control theory for the flexible system governed by the partial differential equation [Eq. (7)]. In this section, the shape adjusting is modelled using the finite element method (FEM), which is a numerical approximate approach to present the dynamic shape-control process.

4.1. Structural dynamics

The dynamic equation of the flexible space structure can be spatially discretized using the FEM as:

$$\boldsymbol{M}\ddot{\boldsymbol{q}} + \boldsymbol{G}\dot{\boldsymbol{q}} + \boldsymbol{K}\boldsymbol{q} = \boldsymbol{f} \tag{34}$$

where $\boldsymbol{q}$ are the total general coordinates of the discrete system for $\boldsymbol{w}(\boldsymbol{r}, t)$. The matrices $\boldsymbol{M}, \boldsymbol{G}$ and $\boldsymbol{K}$ are corresponding to the operators $\mathcal{M}, \mathcal{G}$ and $\mathcal{K}$ respectively. The term $\boldsymbol{f}$ is the total force and its specific form will be given later.

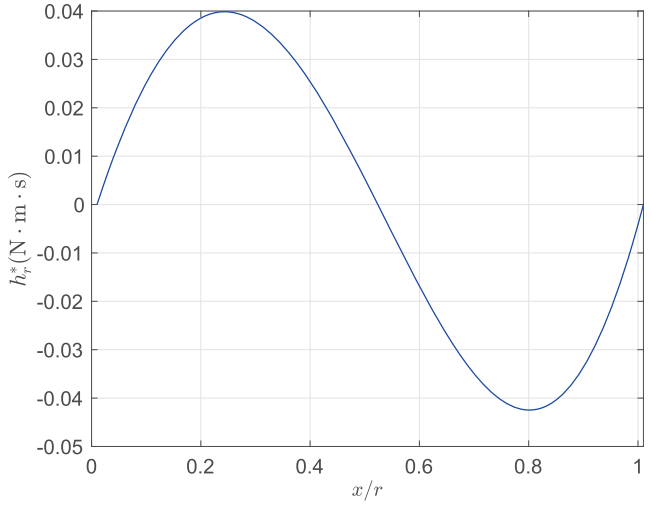

Fig. 5. Optimal gyricity distribution.

The specific elemental configuration for the circular flexible space structure using the FEM is given in the Appendix.

In order to demonstrate the active shape control process comprehensively, the in-plane displacement of the flexible structure will be considered. Thus, the elastic deformation $\boldsymbol{u}_e$ is hereinafter written as $\boldsymbol{u}_e = [u_r, v_\theta, w_e]^\top$ where u_r and v_θ are the in-plane displacements and w_e is the vertical displacement. Based on the theory of the FEM (Petyt, 2010), one uses

$$\boldsymbol{u}_e = \boldsymbol{\Delta}\boldsymbol{q}_e(t) \tag{35}$$

where $\boldsymbol{\Delta}$ are the shape functions and $\boldsymbol{q}_e$ is a column vector of all of the elements' general coordinates $\boldsymbol{q}_{ee}$. More details about the shape function and the general coordinates are referred to the Appendix.

The specific form of the matrix $\boldsymbol{M}$ is given by

$$\boldsymbol{M} = \begin{bmatrix} \boldsymbol{M}_{rr} & \boldsymbol{M}_{re} \\ \boldsymbol{M}_{re}^\top & \boldsymbol{M}_{ee} \end{bmatrix} \tag{36}$$

Here,

$$\boldsymbol{M}_{rr} = \begin{bmatrix} m\boldsymbol{1} & -(\int_V \boldsymbol{r}\mathrm{d}m)^\times \\ (\int_V \boldsymbol{r}\mathrm{d}m)^\times & \boldsymbol{I} \end{bmatrix} \tag{37}$$

where m is the mass, $\boldsymbol{I}$ is the moment of inertia of the flexible space structure and $\boldsymbol{1}$ is the identity matrix. The rigid-elastic coupling matrix $\boldsymbol{M}_{re}$ is given by (Hughes and D'Eleuterio, 1986)

$$\boldsymbol{M}_{re} = \begin{bmatrix} \mathrm{row}\{\boldsymbol{P}_\alpha\} \\ \mathrm{row}\{\boldsymbol{H}_\alpha\} \end{bmatrix}, \qquad \boldsymbol{P}_\alpha = \int_V \boldsymbol{\Delta}\mathrm{d}m, \qquad \boldsymbol{H}_\alpha = \int_V \boldsymbol{\rho}^\times \boldsymbol{\Delta}\mathrm{d}m \tag{38}$$

The global mass matrix $\boldsymbol{M}_{ee}$ can be assembled by the elemental mass matrix $\boldsymbol{m}_{ee}$ which is given by:

$$\boldsymbol{m}_{ee} = \iint_{A_e} \Delta_e^\top \Delta_e \,\mathrm{d}m \tag{39}$$

where Δ_e is the elemental shape function shown in the Appendix.

Since we consider the in-plane displacement u_v and v_θ, the potential energy of the flexible space structure is written in two parts as (Timoshenko and Woinowsky-Krieger, 1959)

$$U = U_\mathrm{e} + U_\mathrm{in} \tag{40}$$

Here,

$$\begin{aligned} U_e = \tfrac{D}{2} \iint_{A_e} & \left[\left(\tfrac{\partial^2 w_e}{\partial r^2} + \tfrac{1}{r}\tfrac{\partial w_e}{\partial r} + \tfrac{1}{r^2}\tfrac{\partial^2 w_e}{\partial \theta^2} \right)^2 \right. \\ & -2(1-\nu)\tfrac{\partial^2 w_e}{\partial r^2}\left(\tfrac{1}{r}\tfrac{\partial w_e}{\partial r} + \tfrac{1}{r^2}\tfrac{\partial^2 w_e}{\partial \theta^2} \right) \\ & \left. +2(1-\nu)\left(\tfrac{1}{r}\tfrac{\partial^2 w_e}{\partial r \partial \theta} - \tfrac{1}{r^2}\tfrac{\partial w_e}{\partial \theta} \right)^2 \right] r\mathrm{d}r\mathrm{d}\theta \end{aligned} \tag{41}$$

and

$$U_{in} = \iint_{A_e} (\sigma_{rr}\epsilon_{rr} + \sigma_{\theta\theta}\epsilon_{\theta\theta} + \tau_{r\theta}\gamma_{r\theta}) r \mathrm{d}r\mathrm{d}\theta \tag{42}$$

where

$$\epsilon_{rr} = \frac{\partial u_r}{\partial r} \tag{43a}$$

$$\epsilon_{\theta\theta} = \frac{1}{r}\frac{\partial v_\theta}{\partial \theta} + \frac{u_r}{r} \tag{43b}$$

$$\gamma_{r\theta} = \frac{1}{2}\left[\frac{1}{r}\frac{\partial u_r}{\partial \theta} + \frac{\partial v_\theta}{\partial r} - \frac{v_\theta}{r}\right] \tag{43c}$$

$$\sigma_{rr} = \frac{E}{1-\nu^2}(\epsilon_{rr} + \nu\epsilon_{\theta\theta}) \tag{43d}$$

$$\sigma_{\theta\theta} = \frac{E}{1-\nu^2}(\epsilon_{\theta\theta} + \nu\epsilon_{rr}) \tag{43e}$$

$$\tau_{r\theta} = \frac{E}{2(1+\nu)}\gamma_{r\theta} \tag{43f}$$

In this way, the stiffness matrix $\boldsymbol{K}_{ee}$ in the FEM can be obtained from

$$U = \frac{1}{2}\boldsymbol{q}_e^\top \boldsymbol{K}_{ee}\boldsymbol{q}_e \tag{43}$$

The stiffness matrix $\boldsymbol{K}$ in Eq. (34) is given by

$$\boldsymbol{K} = \begin{bmatrix} \boldsymbol{0} & \boldsymbol{0} \\ \boldsymbol{0} & \boldsymbol{K}_{ee} \end{bmatrix} \tag{44}$$

In Eq. (34), the specific form of $\boldsymbol{G}$ can be written as

$$\boldsymbol{G} = \int_V \tilde{\boldsymbol{\Lambda}}^\top \mathcal{G}\tilde{\boldsymbol{\Lambda}}\mathrm{d}V \tag{45}$$

where

$$\tilde{\boldsymbol{\Lambda}} = \begin{bmatrix} \boldsymbol{1} \\ -\boldsymbol{r}^\times \\ \boldsymbol{\Lambda} \end{bmatrix} \tag{46}$$

Furthermore, the matrix $\boldsymbol{G}$ can be decomposed as

$$\boldsymbol{G} = \begin{bmatrix} \boldsymbol{G}_{rr} & \boldsymbol{G}_{r\omega} & \boldsymbol{G}_{re} \\ \boldsymbol{G}_{r\omega}^\top & \boldsymbol{G}_{\omega\omega} & \boldsymbol{G}_{\omega e} \\ \boldsymbol{G}_{re}^\top & \boldsymbol{G}_{\omega e}^\top & \boldsymbol{G}_{ee} \end{bmatrix} \tag{47}$$

where

$$\boldsymbol{G}_{rr} = \int_V \boldsymbol{1}(-\mathbf{curl}\boldsymbol{h}_s^\times \mathbf{curl})\boldsymbol{1}\,\mathrm{d}V = \boldsymbol{0} \tag{49a}$$

$$\boldsymbol{G}_{r\omega} = \int_V \boldsymbol{1}(-\mathbf{curl}\boldsymbol{h}_s^\times \mathbf{curl})(-\boldsymbol{r}^\times)\,\mathrm{d}V = \boldsymbol{0} \tag{49b}$$

$$\boldsymbol{G}_{re} = \int_V \boldsymbol{1}(-\mathbf{curl}\boldsymbol{h}_s^\times \mathbf{curl})\boldsymbol{\Delta}\,\mathrm{d}V = \boldsymbol{0} \tag{49c}$$

and

$$\begin{aligned} \boldsymbol{G}_{\omega\omega} &= \textstyle\int_V (-\boldsymbol{r}^\times)(-\mathbf{curl}\boldsymbol{h}_s^\times)\,\mathrm{d}V \\ &= h\textstyle\iint_A \boldsymbol{h}_s^\times r\mathrm{d}r\mathrm{d}\theta \\ &= h\cdot 2\pi\textstyle\int \boldsymbol{h}_s^\times r\mathrm{d}r \end{aligned} \tag{50}$$

In Eq. (50), h is the thickness of the flexible space structure. According to the optimal gyricity distribution (Fig. (5)) yielded from Section 3, it can be verified that

$$\int_{r_h}^{R} h_r^* r\,\mathrm{d}r = 0 \tag{51}$$

That is

$$\boldsymbol{G}_{\omega\omega} = \boldsymbol{0} \tag{52}$$

Also, in Eq. (47), the term $\boldsymbol{G}_{we}$ is given by

$$\boldsymbol{G}_{we} = \int_V (\mathbf{curl}^\times \boldsymbol{\Delta})^\top \boldsymbol{h}_s^\times \mathrm{d}V \tag{53}$$

As mentioned in Remark 1, the gyricity distribution is the source of control force implementing the shape deformation of the flexible structure. The force $\boldsymbol{f}_h$, which is provided by the optimal gyricity distribution developed in Section 3, is written as

$$\boldsymbol{f}_h(\boldsymbol{r}, t) = -\mathcal{G}\dot{\boldsymbol{w}} \tag{54}$$

According Eq. (6), we have

$$\boldsymbol{f}_h = -\mathcal{G}(-\boldsymbol{r}^\times\dot{\boldsymbol{\theta}} + \dot{\boldsymbol{u}}_e) = \mathcal{G}\boldsymbol{r}^\times\dot{\boldsymbol{\theta}} - \mathcal{G}\dot{\boldsymbol{u}}_e \tag{55}$$

where the term $\mathcal{G}\dot{\boldsymbol{u}}_e$ is the source of the matrix $\boldsymbol{G}_{ee}$. According to the FEM, the corresponding elemental gyricity matrix $\boldsymbol{g}_{ee}$ is given by

$$\boldsymbol{g}_{ee} = -\int_V (\mathbf{curl}\Delta_e)^\top \boldsymbol{h}_s^\times (\mathbf{curl}\Delta_e)\mathrm{d}V \tag{56}$$

where Δ_e is the element shape function. The global gyricity matrix $\boldsymbol{G}_{ee}$ is constructed by the standard assembling procedure of the FEM using the elemental gyricity matrix $\boldsymbol{g}_{ee}$.

The term $\mathcal{G}\boldsymbol{r}^\times\dot{\boldsymbol{\theta}}$ is the source of modal force $\boldsymbol{f}_e$ which can be calculated as:

$$\boldsymbol{f}_e = \int_V \boldsymbol{\Delta}^\top \mathbf{curl}\,\boldsymbol{h}_s\dot{\boldsymbol{\theta}}\mathrm{d}V \tag{57}$$

Since the direction of the optimal gyricity distribution h_r^* is radial, the direction of $\boldsymbol{f}_e$ is along with z-axis in the rotating field to balance the stiffness of the structure, as mentioned previously. Hence, the elemental force matrix $\boldsymbol{f}_{ee}$ can be written as

$$\boldsymbol{f}_{ee} = \iint_{A_e} \Delta_e^\top \Omega\left(\frac{1}{r} + \frac{\partial}{\partial r}\right) h_r r\mathrm{d}r\mathrm{d}\theta \tag{58}$$

The global force matrix $\boldsymbol{f}_e$ is assembled using $\boldsymbol{f}_{ee}$ and the standard procedure of the FEM. In Eq. (34), the total force $\boldsymbol{f}$ is given by

$$\boldsymbol{f} = \begin{bmatrix} \boldsymbol{f}_t \\ \boldsymbol{\tau} \\ \boldsymbol{f}_e \end{bmatrix} \tag{59}$$

where $\boldsymbol{f}_t$ and $\boldsymbol{\tau}$ are the external force and torque corresponding to the translation and rotation of the structure respectively. Assuming that the translation of the flexible space structure is not considered, this implies that

$\boldsymbol{f}_t = [0,0,0]^\top$. Evoking Section 3, the radial gyricity distribution h_r is used to generate the distributed forces to change the shape of the flexible structure when it is rotating about its z-axis. The torque $\boldsymbol{\tau}$ in Eq. (59) is the source of this rotation so that

$$\boldsymbol{\tau} = \begin{bmatrix} 0 \\ 0 \\ I_z\dot{\Omega} \end{bmatrix} \tag{60}$$

where I_z is the moment of inertia of the flexible structure in the z-axis and Ω is the angular velocity about the z-axis.

4.2. Numerical simulation

The simulation of the active shape control process of the circular flexible space structure is implemented here. The eigenvalue problem of Eq. (34) without the consideration of the force term $\boldsymbol{f}$ and gyricity term $\boldsymbol{G\dot{q}}$ can be written as

$$-\omega_\alpha^2 \boldsymbol{M}\boldsymbol{q}_\alpha + \boldsymbol{K}\boldsymbol{q}_\alpha = \boldsymbol{0}, \qquad \alpha = 1,2,3,\cdots \tag{61}$$

where ω_α are the eigenvalues and $\boldsymbol{q}_\alpha$ are the corresponding eigenvectors which satisfy

$$\boldsymbol{q}_\alpha^\top \boldsymbol{M}\boldsymbol{q}_\beta = \delta_{\alpha\beta}, \qquad \boldsymbol{q}_\alpha^\top \boldsymbol{K}\boldsymbol{q}_\beta = \omega_\alpha^2\delta_{\alpha\beta} \tag{62}$$

Here, $\delta_{\alpha\beta}$ is the Kronecker delta ($\delta_{\alpha\beta} = 1$ when $\alpha = \beta$ and $\delta_{\alpha\beta} = 0$ when $\alpha \neq \beta$).

The solution of Eq. (61) can be approximated as

$$\boldsymbol{q}(t) = \sum_{\alpha=1}^{N_t} \boldsymbol{q}_\alpha \eta_\alpha(t) \tag{63}$$

where N_t is the truncated order and $\eta_\alpha(t), \alpha = 1,2,3,\cdots$, are the modal coordinates. In this way, Eq. (61) can be written as

$$\boldsymbol{q}_\beta^\top \boldsymbol{M}\sum_{\alpha=1}^{N_t}\boldsymbol{q}_\alpha\ddot{\eta}_\alpha(t) + \boldsymbol{q}_\beta^\top \boldsymbol{G}\sum_{\alpha=1}^{N_t}\boldsymbol{q}_\alpha\dot{\eta}_\alpha(t) + \boldsymbol{q}_\beta^\top \boldsymbol{K}\sum_{\alpha=1}^{N_t}\boldsymbol{q}_\alpha\eta_\alpha(t) = \boldsymbol{q}_\beta^\top \boldsymbol{f}, \beta = 1,2,3,\cdots \tag{64}$$

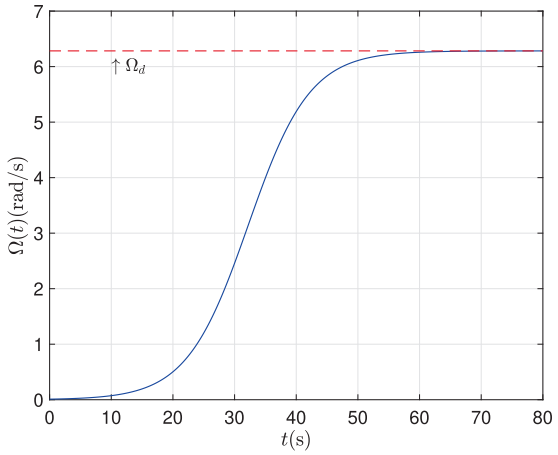

Fig. 6. Angular velocity around $z$axis vs time.

To conduct the numerical simulation, the physical parameters of the flexible space structure are described as follows. The elastic modulus is $E = 70\,\text{GPa}$. The Poisson ratio is $\gamma = 0.3$. The density is $2.7 \times 10^3\,\text{kg/m}^3$. The thickness is $h = 0.01\text{m}$. The outer radius of the structure is $r = 1.01\text{m}$. The radius of the central hole is $r_h = 0.01\text{m}$. The flexible space structure is rotating about its z-axis with angular velocity Ω given by

$$\Omega(t) = \frac{\Omega_d}{1 + (\frac{\Omega_d}{a} - 1)e^{-\lambda t}} \tag{65}$$

where Ω_d is the final value of $\Omega(t)$, and a and λ are two constants. Here, they are taken as $\Omega_d = 2\pi\,\text{rad/s}, a = 0.1\,\text{rad/s}$ and $\lambda = 0.2s^{-1}$. The evolution of Ω is shown in Fig. 6.

Using the angular velocity shown in Fig. 6 and the optimal gyricity distribution h_r^*, the model force $\boldsymbol{f}_e$ can be calculated by Eq. (57). The shape of the flexible structure is deformed by the distributed force applied on all points on this structure rather than any one. The time responses of the distributed forces are hard to be depicted by figures. Alternatively, its illustration is replaced by the optimal gyricity distribution, the core part of the distributed force,

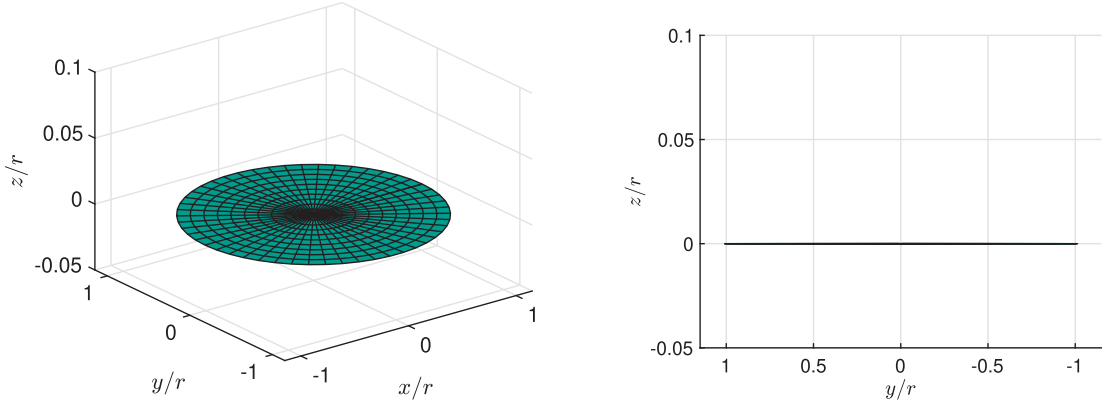

(a) Three-dimensional shape (b) Two-dimensional shape

Fig. 7. Shape of the flexible structure when $t = 0$s.

which has already been depicted in Fig. 5. As addressed in Section 3, in fact, the gyricity distribution is regarded as the equivalent control input of the system.

The simulation results of the shape adjusting process are shown from Fig. 7 ($t = 0$ s) to Fig. 13 ($t = 60$ s) in a nondimensional way. Note that the left side of each figure shows the three-dimentional shape of the flexible structure during the shape deformation process, and the right side of each figure manifests the two-dimensional shape looking from the x axis at the $y - z$ plane. At the initial stage of deformation ($t = 0$ s), the shape of the flexible structure is a plane-plate which is shown in Fig. 7. As time goes on, the shape is

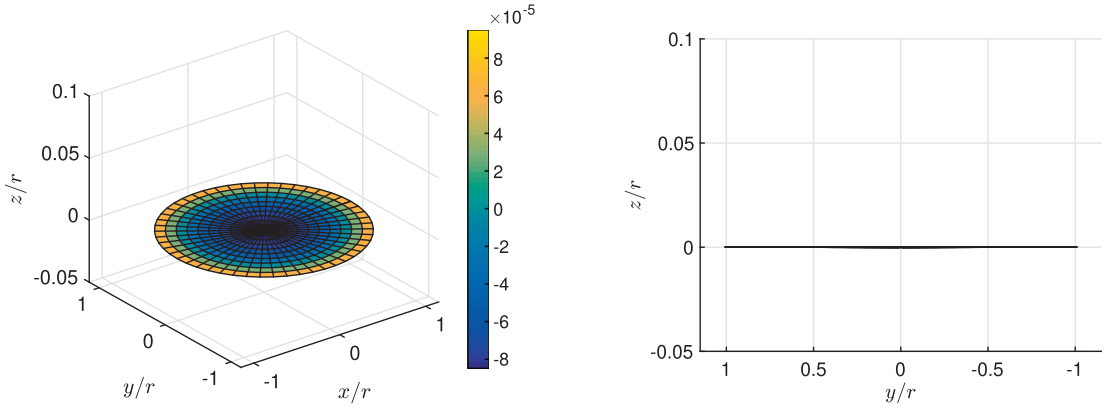

(a) Three-dimensional shape (b) Two-dimensional shape

Fig. 8. Shape of the flexible structure when $t = 10$s.

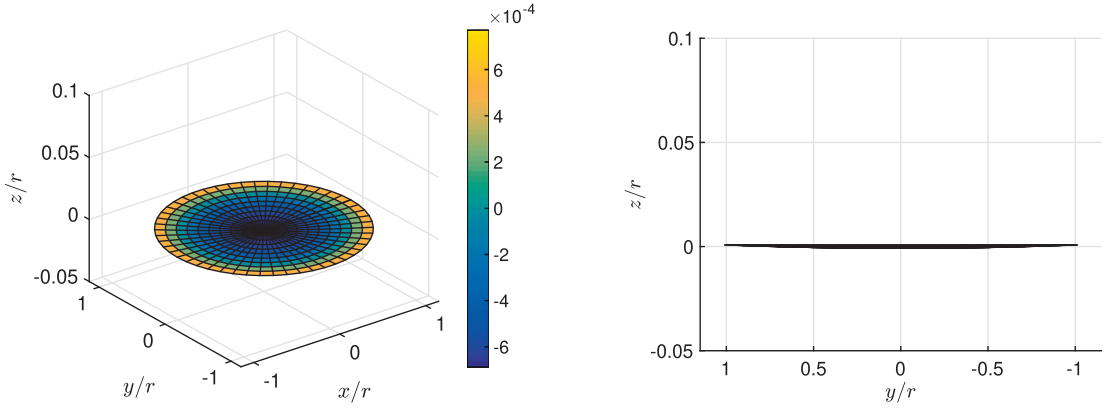

(a) Three-dimensional shape (b) Two-dimensional shape

Fig. 9. Shape of the flexible structure when $t = 20$s.

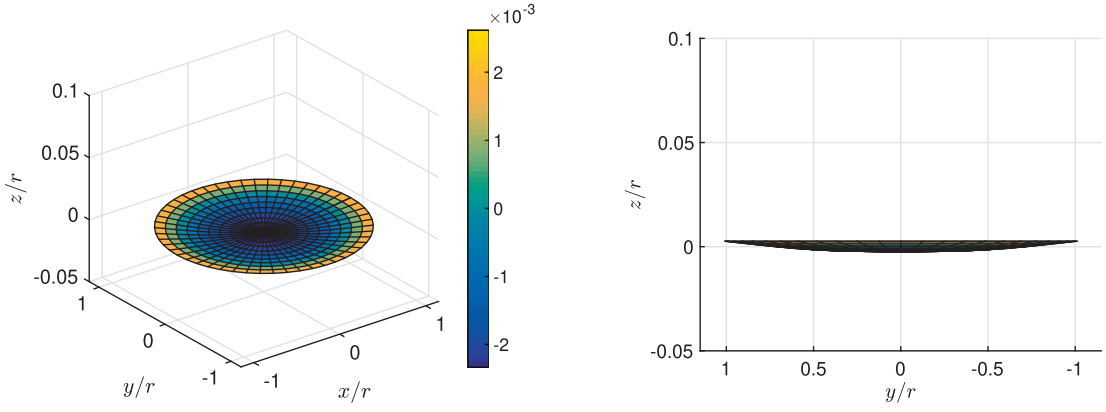

(a) Three-dimensional shape (b) Two-dimensional shape

Fig. 10. Shape of the flexible structure when $t = 30$s.

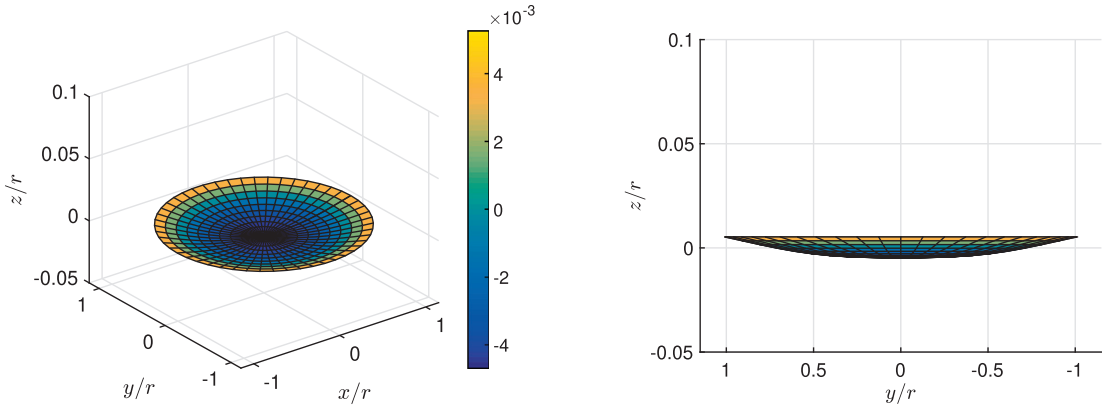

(a) Three-dimensional shape (b) Two-dimensional shape

Fig. 11. Shape of flexible structure when $t = 40$s.

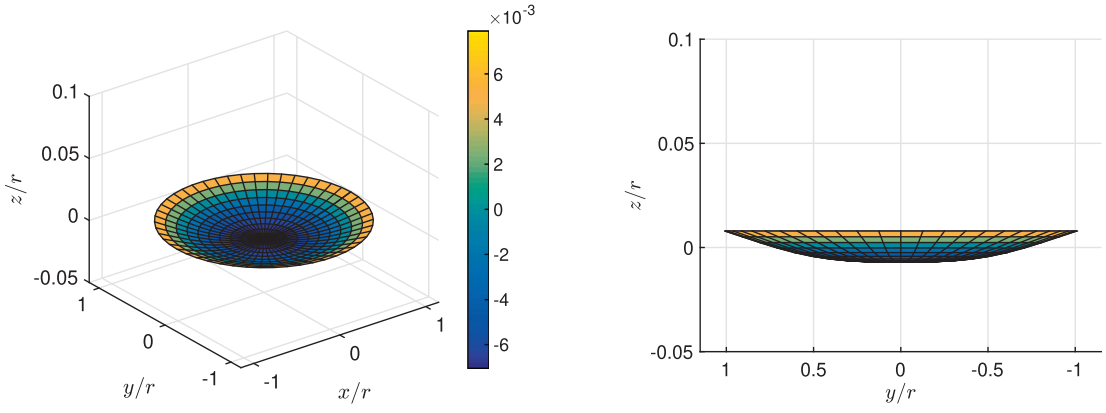

(a) Three-dimensional shape (b) Two-dimensional shape

Fig. 12. Shape of flexible structure when $t = 50$s.

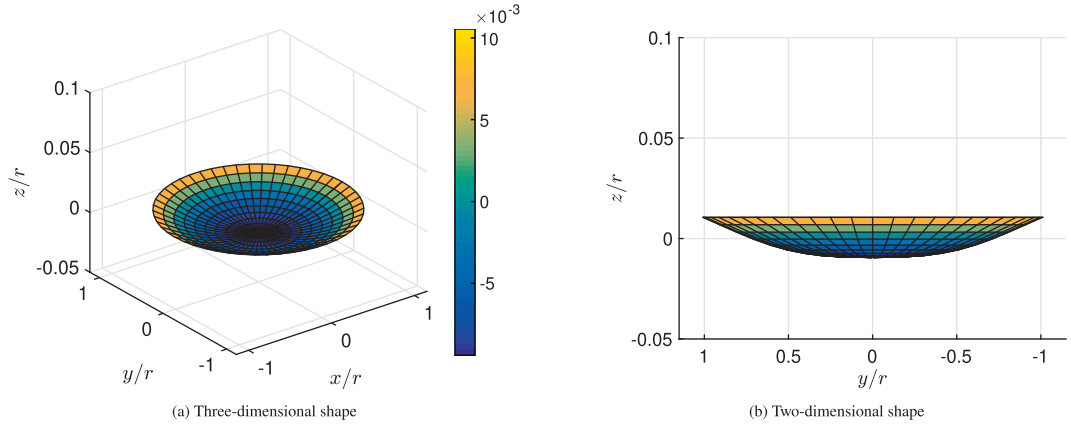

(a) Three-dimensional shape (b) Two-dimensional shape

Fig. 13. Shape of flexible structure when $t = 60$s.

approaching the desired paraboloidal shape, which are depicted in Figs. 8–13. From these results, it can be seen that the shape of the flexible structure is changed by the distributed forces produced from the optimal gyricity distribution h_r^* when the structure is rotating about its z-axis. A point at the edge of the flexible structure is selected as a representative, and the time response of its vertical displacement is shown in Fig. 15. It can be seen that the vertical displacement of this point is continuously increasing until the paraboloidal shape of the flexible structure is formed. No structural oscillation appears during the entire shape control process. To evaluate the performance of the optimal gyricity, the comparison between the expected shape and the real shape is illustrated at Fig. 14. The real shape is not identical with the expected shape. The reason for the discrepancy is that the derivation of the optimal gyricity distribution in Section 3 does not use the in-plane structural dynamics but the simulation does. To

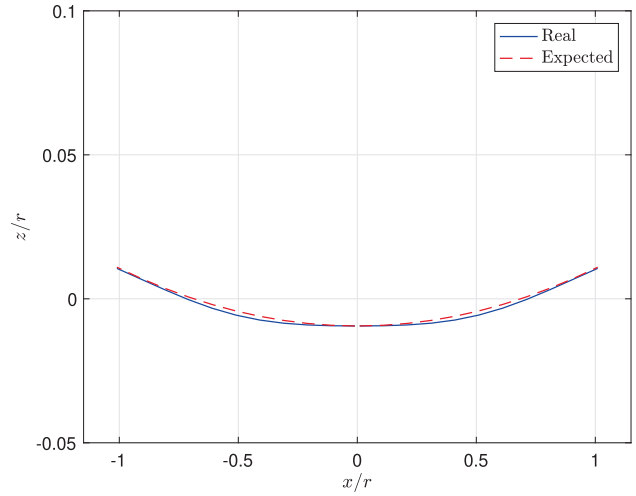

Fig. 14. Comparison between the expected shape and the real shape (t = 60s).

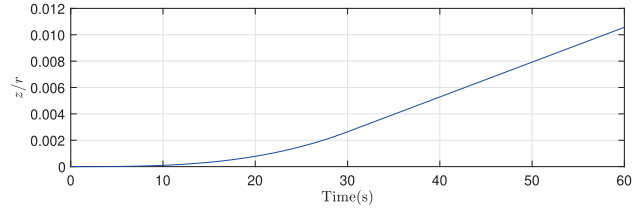

Fig. 15. Time response of a point at the edge of the flexible structure.

quantize the discrepancy during the entire shape deformation process, a notion of root-mean-square-like error $E(t)$ presented in Zong et al. (2016) was utilized in this paper, and it is given by

$$E(t) \triangleq \sqrt{\frac{\left[z_r^i(t) - z_d^i\right]^2}{n_{\text{node}}}} \tag{66}$$

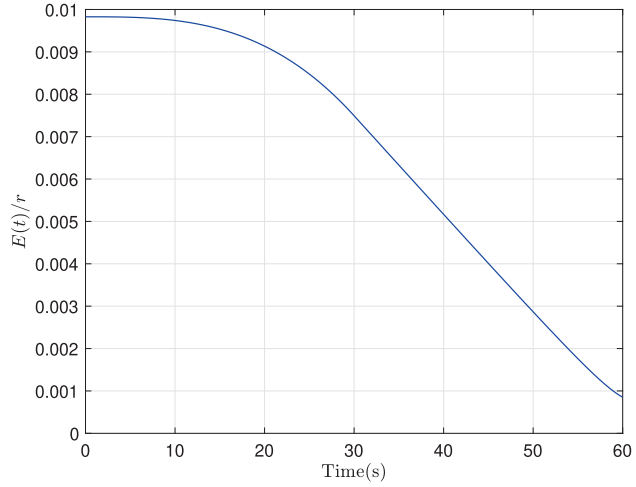

Fig. 16. Time response of the root-mean-square-like error $E(t)$.

where $z_{r_i}(t)$ is the real vertical displacement of node i at the time instant t and z_d^i is the desired vertical displacement of node i. n_{node} is the total number of all nodes used in FEM. The time response of $E(t)$ is depicted in Fig. 16 where the shape discrepancy is continuously decreasing, although there is still a small discrepancy existing at the final stage. Denote the maximum vertical displacement of the structure during the simulation as $z_{\max}$. The relative error at the final stage is $E(t_f)/z_{\max} \times 100\% = 4.26\%$($t_f$ is the final time of simulation), which is relatively small (less than 5%) under the proposed shape control scheme.

5. Conclusions

In this paper, the optimal gyricity distribution has been derived using optimal control theory for the systems described by partial differential equations. The shape of the circular flexible space structure is deformed by the distributed forces which are triggered by the optimal gyricity distribution in a rotating field. The dynamics of the shape control is presented using the finite element method, and the forms of the gyricity matrix and modal force vector are given explicitly. Numerical simulation demonstrates the effectiveness of the proposed active shape control method, where the shape is deformed from a plane plate to a paraboloidal shape.

Declaration of Competing Interest

The authors declare that they have no known competing financial interests or personal relationships that could have appeared to influence the work reported in this paper.

Appendix A. Elemental configuration of the flexible space structure

The dynamic equation of the circular flexible space structure is established using the FEM. The following formulation is mainly based on Petyt (2010). The circular flexible space structure is regarded as a thin plate and its mesh configuration is shown in Fig. 17. A rectangular-like element is used to approximate each element in the mesh configuration. Given the structure is a circular shape with a tiny hole at the center, the cylindrical coordinate system is used with the FEM. The polar coordinate part (r, θ) lies within the plate plane and its original point is fixed at the plate's geometric center (Note that the notation r and θ are herein used for the formulation of the FEM in this Appendix and are different from the same notations used in the former parts of this paper). The z-axis is perpendicular to the (r, θ) coordinate to calibrate all nodes' vertical displacements. Four nodes are considered for each rectangular-like element which has the inside radius r_1, outside radius r_2, subtends angle β and straight length r_e. For the sake of simplicity, the vertical displacement w_e and its two affiliated rotation $w_{er} = \partial w_e/\partial r$ and $w_{e\theta} = \partial w_e/\partial\theta$ of

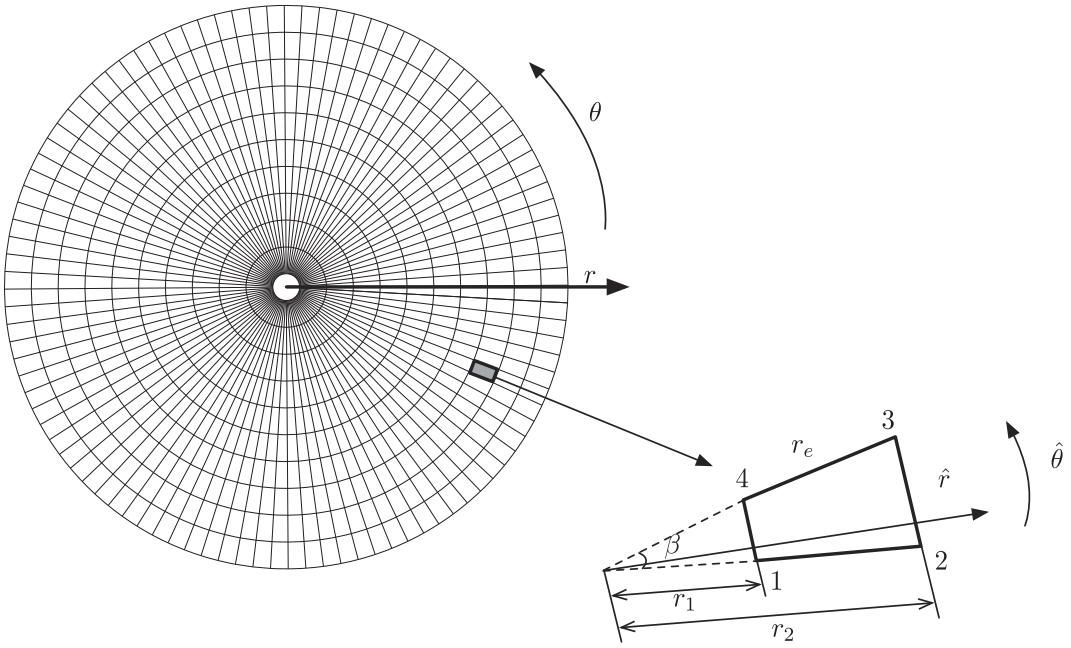

Fig. 17. Finite element mesh and a single element.

a node are discussed at first and in-plane displacements are analyzed later. In the mesh element, a local polar coordinate $(\hat{r},\hat{\theta})$ is used and it can be converted to the global polar coordinate (r,θ) by:

$$\begin{aligned} r &= r_h + (i-1)r_e + r_e\hat{r} \\ \theta &= \theta_j + \beta\hat{\theta} \end{aligned} \tag{67}$$

where i and θ_j are the position indices for the element in the mesh configuration and r_h is the central hole's radius. The rotations w_{er} and $w_{e\theta}$ can be expressed as

$$w_r = \frac{1}{r_e}\frac{\partial w}{\partial \hat{r}} = \frac{w_{\hat{r}}}{r_e}, w_\theta = \frac{1}{\beta}\frac{\partial w}{\partial \hat{\theta}} = \frac{w_{\hat{\theta}}}{\beta} \tag{68}$$

The vertical displacement w_e can be approximated by a twelve-term polynomial as

$$\begin{aligned} w_e(\hat{r},\hat{\theta},t) &= \alpha_1 + \alpha_2\hat{r} + \alpha_3\hat{\theta} + \alpha_4\hat{r}^2 + \alpha_5\hat{r}\hat{\theta} + \alpha_6\hat{\theta}^2 + \alpha_7\hat{r}^3 + \alpha_8\hat{r}^2\hat{\theta} \\ &\quad + \alpha_9\hat{r}\hat{\theta}^2 + \alpha_{10}\hat{\theta}^3 + \alpha_{11}\hat{r}^3\hat{\theta} + \alpha_{12}\hat{r}\hat{\theta}^3 \\ &= \boldsymbol{C}(\hat{r},\hat{\theta})\boldsymbol{\alpha}(t) \end{aligned} \tag{69}$$

Here,

$$\boldsymbol{C}(\hat{r},\hat{\theta}) = [1 \;\; \hat{r} \;\; \hat{\theta} \;\; \hat{r}^2 \;\; \hat{r}\hat{\theta} \;\; \hat{\theta}^2 \;\; \hat{r}^3 \;\; \hat{r}^2\hat{\theta} \;\; \hat{r}\hat{\theta}^2 \;\; \hat{\theta}^3 \;\; \hat{r}^3\hat{\theta} \;\; \hat{r}\hat{\theta}^3] \tag{70}$$

and

$$\boldsymbol{\alpha}(t) = [\alpha_1(t) \quad \alpha_2(t) \quad \cdots \quad \alpha_{12}(t)]^\top \tag{71}$$

The vertical displacement and two rotations of the node i are described as:

$$\begin{bmatrix} w_{ei} \\ w_{eri} \\ w_{e\theta i} \end{bmatrix} = \begin{bmatrix} 1 & \hat{r}_i & \hat{\theta}_i & \hat{r}_i\hat{\theta}_i & \hat{r}_i^2 & \hat{\theta}_i^2 & \hat{r}_i^2\hat{\theta}_i & \hat{r}_i\hat{\theta}_i^2 & \hat{r}_i^3 & \hat{\theta}_i^3 & \hat{r}_i^3\hat{\theta}_i & \hat{r}_i\hat{\theta}_i^3 \\ 0 & 1 & 0 & \hat{\theta}_i & 2\hat{r}_i & 0 & 2\hat{r}_i\hat{\theta}_i & \hat{\theta}_i^2 & 3\hat{r}_i & 0 & 3\hat{r}_i^2\hat{\theta}_i & \hat{\theta}_i^3 \\ 0 & 0 & 1 & \hat{r}_i & 0 & 2\hat{\theta}_i & \hat{r}_i^2 & 2\hat{r}_i\hat{\theta}_i & 0 & 3\hat{\theta}_i^2 & \hat{r}_i^3 & 3\hat{r}_i\hat{\theta}_i^2 \end{bmatrix} \boldsymbol{\alpha}(t) \tag{72}$$

In the local polar coordinate system $(\hat{r},\hat{\theta})$, the coordinates of an element's four nodes are 1 $(0,0)$, 2 $(1,0)$, 3 $(1,1)$, and 4 $(0,1)$. Hence, the degrees of freedom for a single element $\boldsymbol{q}_{ee}$ are written as:

$$\boldsymbol{q}_{ee} = [w_{e1} \;\; r_e w_{er1} \;\; \beta w_{e\theta 1} \;\; \cdots \;\; w_{e4} \;\; r_e w_{er4} \;\; \beta w_{e\theta 4}]^\top = \boldsymbol{A}_e\boldsymbol{\alpha}(t) \tag{73}$$

where

$$\boldsymbol{A}_e = \begin{bmatrix} 1 & 0 & 0 & 0 & 0 & 0 & 0 & 0 & 0 & 0 & 0 & 0 \\ 0 & 1 & 0 & 0 & 0 & 0 & 0 & 0 & 0 & 0 & 0 & 0 \\ 0 & 0 & 1 & 0 & 0 & 0 & 0 & 0 & 0 & 0 & 0 & 0 \\ 1 & 1 & 0 & 0 & 1 & 0 & 0 & 0 & 1 & 0 & 0 & 0 \\ 0 & 1 & 0 & 0 & 2 & 0 & 0 & 0 & 3 & 0 & 0 & 0 \\ 0 & 0 & 1 & 1 & 0 & 0 & 1 & 0 & 0 & 0 & 1 & 0 \\ 1 & 1 & 1 & 1 & 1 & 1 & 1 & 1 & 1 & 1 & 1 & 1 \\ 0 & 1 & 0 & 1 & 2 & 0 & 2 & 1 & 3 & 0 & 3 & 1 \\ 0 & 0 & 1 & 1 & 0 & 2 & 1 & 2 & 0 & 3 & 1 & 3 \\ 1 & 0 & 1 & 0 & 0 & 1 & 0 & 0 & 0 & 1 & 0 & 0 \\ 0 & 1 & 0 & 1 & 0 & 0 & 0 & 1 & 0 & 0 & 0 & 1 \\ 0 & 0 & 1 & 0 & 0 & 2 & 0 & 0 & 0 & 3 & 0 & 0 \end{bmatrix} \tag{74}$$

Substituting Eqs. (73) and (74) into Eq. (69) gives

$$\begin{aligned} w_e(r,\theta,t) &= \boldsymbol{C}(r,\theta)\boldsymbol{\alpha}(t) = \boldsymbol{C}(r,\theta)\boldsymbol{A}_e^{-1}\boldsymbol{q}_{ee}(t) \\ &= \boldsymbol{N}(r,\theta)\boldsymbol{q}_{we}(t) \end{aligned} \tag{75}$$

where

$$\boldsymbol{N}(r,\theta) = \boldsymbol{C}(r,\theta)\boldsymbol{A}_e^{-1} = [\boldsymbol{N}_1,\boldsymbol{N}_2,\boldsymbol{N}_3,\boldsymbol{N}_4] \tag{76}$$

When the in-plane displacement u_r and v_θ are considered, the elastic deformation $\boldsymbol{u}_e = [u_r, v_\theta, w_e]^\top$ can be reformed based on the theory of the FEM as

$$\boldsymbol{u}_e = \Delta_e \boldsymbol{q}_{ee} \tag{77}$$

where $\boldsymbol{q}_{ee} = \left[\boldsymbol{q}_{u_r}, \boldsymbol{q}_{v_\theta}, \boldsymbol{q}_{w_e}\right]^\top$ and Δ_e is the elemental shape function which is given by:

$$\Delta_e = \begin{bmatrix} \boldsymbol{N}_1 & \boldsymbol{0} & \boldsymbol{N}_2 & \boldsymbol{0} & \boldsymbol{N}_3 & \boldsymbol{0} & \boldsymbol{N}_4 & \boldsymbol{0} & \boldsymbol{0} \\ \boldsymbol{0} & \boldsymbol{N}_1 & \boldsymbol{0} & \boldsymbol{N}_2 & \boldsymbol{0} & \boldsymbol{N}_3 & \boldsymbol{0} & \boldsymbol{N}_4 & \boldsymbol{0} \\ \boldsymbol{0} & \boldsymbol{0} & \boldsymbol{0} & \boldsymbol{0} & \boldsymbol{0} & \boldsymbol{0} & \boldsymbol{0} & \boldsymbol{0} & \boldsymbol{N} \end{bmatrix} = \begin{bmatrix} \boldsymbol{N}_{u_r} \\ \boldsymbol{N}_{v_\theta} \\ \boldsymbol{N}_{w_e} \end{bmatrix} \tag{78}$$

References

Austin, F., Rossi, M.J., Van Nostrand, W., Knowles, G., Jameson, A., 1994. Static shape control for adaptive wings. AIAA J. 32, 1895–1901. https://doi.org/10.2514/3.12189.

Balas, M.J., 1985. Optimal quasi-static shape control for large aerospace antennae. J. Optim. Theory Appl. 46, 153–170. https://doi.org/10.1007/bf00938421.

Borggräfe, A., Heiligers, J., Ceriotti, M., McInnes, C., 2013. Shape-changing solar sails for novel mission applications. In: 64th International Astronautical Congress 2013. IAF, Beijing, China, pp. 1–10.

Chee, S.A., Damaren, C.J., 2015. Optimal gyricity distribution for space structure vibration control. J. Guidance, Control, Dyn. 38, 1218–1228. https://doi.org/10.2514/1.g000293.

Damaren, C.J., D'Eleuterio, G.M.T., 1989. Optimal control of large space structures using distributed gyricity. J. Guidance, Control, Dyn. 12, 723–731. https://doi.org/10.2514/3.20467.

Damaren, C.J., D'Eleuterio, G.M.T., 1991. Controllability and observability of gyroelastic vehicles. J. Guidance, Control, Dyn. 14, 886–894. https://doi.org/10.2514/3.20728.

D'Eleuterio, G.M.T., Hughes, P.C., 1984. Dynamics of gyroelastic continua. J. Appl. Mech. 51, 415–422. https://doi.org/10.1115/1.3167634.

D'Eleuterio, G.M.T., Hughes, P.C., 1987. Dynamics of gyroelastic spacecraft. J. Guidance, Control, Dyn. 10, 401–405. https://doi.org/10.2514/3.20231.

Fan, L., Lv, L.-L., Peng, F.-J., Cai, G.-P., 2020. Coupled structural-electromagnetic modeling and analysis of active membrane phased array antenna. Adv. Space Res. 66, 760–770. https://doi.org/10.1016/j.asr.2020.04.049.

Gorinevsky, D., Hyde, T., Cabuz, C., 2001. Distributed shape control of lightweight space reflector structure. In: Proceedings of the 40th IEEE Conference on Decision and Control, vol. 4. IEEE, Orlando, Florida, USA, pp. 3850–3855, https://doi.org/10.1109/cdc.2001.980466.

Hassanpour, S., Heppler, G., 2016. Dynamics of 3d timoshenko gyroelastic beams with large attitude changes for the gyros. Acta Astronaut. 118, 33–48. https://doi.org/10.1016/j.actaastro.2015.09.012.

Hu, T., Gong, S., Mu, J., Li, J., Wang, T., Qian, W., 2016. Switch programming of reflectivity control devices for the coupled dynamics of a solar sail. Adv. Space Res. 57, 1147–1158. https://doi.org/10.1016/j.asr.2015.12.029.

Hu, Y., Vukovich, G., 2005. Active robust shape control of flexible structures. Mechatronics 15, 807–820. https://doi.org/10.1016/j.mechatronics.2005.02.004.

Hughes, P.C., D'Eleuterio, G.M.T., 1986. Modal parameter analysis of gyroelastic continua. J. Appl. Mech. 53, 918–924. https://doi.org/10.1115/1.3171881.

Lions, J.L., 1971. Optimal control of systems governed by partial differential equations. Springer, Berlin.

Liu, J., Fu, Y., Zhang, L., Luo, N., Wang, W., Zhao, D., Wu, Z., 2021. Surface shape control of integrated paraboloid space reflector consisting of sub-reflectors exploiting modulated solar pressure. Adv. Space Res. 67, 1333–1349. https://doi.org/10.1016/j.asr.2020.11.017.

Petyt, M., 2010. Introduction to finite element vibration analysis. Cambridge University Press.

Sanz-Fernandez, J., Saenz, E., de Maagt, P., 2015. A circular polarization selective surface for space applications. IEEE Trans. Antennas Propag. 63, 2460–2470. https://doi.org/10.1109/TAP.2015.2414450.

Silva, O.M., Valentini, F., Cardoso, E.L., 2021. Shape and position preserving design of vibrating structures by controlling local energies through topology optimization. J. Sound Vib. 515, 116478. https://doi.org/10.1016/j.jsv.2021.116478.

Tabata, M., Natori, M., 1996. Active shape control of a deployable space antenna reflector. J. Intell. Mater. Syst. Struct. 7, 235–240. https://doi.org/10.1177/1045389x9600700216.

Takao, Y., Mori, O., Matsushita, M., Okuizumi, N., Satou, Y., Kawaguchi, J., 2022. Active shape control of membrane structures using spin-synchronous vibrations. J. Spacecraft Rock. 59, 295–311. https://doi.org/10.2514/1.A35084.

Timoshenko, S.P., Woinowsky-Krieger, S., 1959. Theory of plates and shells. McGraw-hill.

Xie, Y.M., Shi, H., Alleyne, A., Yang, B.E., 2016. Feedback shape control for deployable mesh reflectors using gain scheduling method. Acta Astronaut. 121, 241–255. https://doi.org/10.1016/j.actaastro.2016.01.005.

Xun, G., Peng, H., Wu, S., Wu, Z., 2018. Active shape adjustment of large cable-mesh reflectors using novel fast model predictive control. J. Aerospace Eng. 31. https://doi.org/10.1061/(asce)as.1943-5525.0000858, 04018038(1-11).

Zhang, J., Xiang, Z., Liu, Y., 2013. Quasi-static shape control of flexible space structures by using heaters. AIAA J. 51, 1003–1007. https://doi.org/10.2514/1.j052155.

Zhou, W., Zhang, Z., Wang, X., Lv, W., Hu, X., 2021. Structure-actuator integrated design of piezo-actuated composite plate wing for active shape control. J. Aerospace Eng. 34, 04021070. https://doi.org/10.1061/(ASCE)AS.1943-5525.0001322.

Zong, Y., Zhang, S., Du, J., Yang, G., Xu, W., Hu, N., 2016. Shape control of cable-network antennas considering the RF performance. IEEE Trans. Antennas Propag. 64, 839–848. https://doi.org/10.1109/tap.2015.2513088.